

## Unoccupied orbitals of 3*d* transition metals in ZnS

V. Pérez-Dieste,<sup>1</sup> J. N. Crain,<sup>1</sup> A. Kirakosian,<sup>1</sup> J. L. McChesney,<sup>1</sup> E. Arenholz,<sup>2</sup> A. T. Young,<sup>2</sup> J. D. Denlinger,<sup>2</sup> D. L. Ederer,<sup>3</sup> T. A. Callcott,<sup>4</sup> S. A. Lopez-Rivera,<sup>5</sup> and F. J. Himpsel<sup>1</sup>

<sup>1</sup>*Department of Physics, University of Wisconsin-Madison, Madison, Wisconsin 53706, USA*

<sup>2</sup>*Advanced Light Source, Lawrence Berkeley National Laboratory, Berkeley, California 94720, USA*

<sup>3</sup>*Physics Department, Tulane University, New Orleans, Louisiana 70118, USA*

<sup>4</sup>*Department of Physics, Knoxville, Tennessee 37996, USA*

<sup>5</sup>*Laboratorio de Física Aplicada, Universidad de los Andes, Merida, Venezuela*

(Received 19 January 2004; revised manuscript received 13 May 2004; published 24 August 2004)

The electronic structure of magnetic impurities in ZnS is determined by near edge x-ray absorption for the 3*d* transition metals Ti, Mn, Fe, Co, Ni embedded in single crystal ZnS. By detecting emitted fluorescence photons instead of electrons it is possible to suppress the background from the host and to eliminate charging problems. The spectra exhibit considerable fine structure, which makes it possible to determine the tetrahedral crystal field 10*Dq* from the multiplet pattern: 10*Dq*=0.5 eV for Mn, 0.7 eV for Fe, 0.7 eV for Co.

DOI: 10.1103/PhysRevB.70.085205

PACS number(s): 75.50.Pp, 78.70.Dm, 71.20.Nr

### I. INTRODUCTION

Magnetic semiconductors have generated interest for a variety of reasons, such as the unique interaction of localized 3*d* transition metal spins with valence and the *sp*-like conduction band states which leads to huge Faraday rotation, *g* factors, and large magnetoresistance.<sup>1</sup> For this reason they have been referred to as “spin amplifiers.” Recently, there has been a flurry of activity to create ferromagnetic semiconductors that would make it possible to merge traditional electronics with magnetoelectronics, where spins are switched instead of charges. For example, one would be able to control a semiconductor device by a magnetic field. While most magnetic semiconductors are antiferromagnetic they can be ferromagnetic as demonstrated by the Mn in GaAs, the system that triggered the interest in electronic applications.<sup>2–5</sup> Curie temperatures  $T_C$  of 110 K have been achieved, and there is a possibility that a  $T_C$  above room temperature can be achieved with special growth conditions or via nanostructured hybrid materials.<sup>6,7</sup> With  $T_C$  above room temperature magnetic semiconductors could become commercially viable. It appears that hosts with small cations and larger band gaps may lead to higher  $T_C$ , for example, GaP, ZnO,<sup>8,9</sup> MnO,<sup>10</sup> and CoO,<sup>11</sup> although exploratory work has not been fully conclusive due to the segregation and alloy formation of transition metals. For further progress it is essential to exclude that possibility. For example, in Cr doped ZnTe, which has a  $T_C$  of 300 K, an analysis of the magnetic circular dichroism spectral shape was performed to confirm the presence of *sp-d* exchange interaction and discard that magnetic precipitates could be responsible of its ferromagnetism.<sup>12</sup> Predictions based on Zener’s model suggest that lighter elements in III-V and II-VI compounds favor higher  $T_C$  at a fixed Mn concentration,<sup>9</sup> but the applicability of this model has been questioned for the case of diamond and possibly a wider class of compounds.<sup>13,14</sup> Therefore, we have explored the electronic structure of Mn and other 3*d* transition metal impurities in ZnS, which has light constituents and exhibits a relatively wide gap of 3.7 eV.

A fairly detailed picture of the interaction between the magnetic impurity and the host has evolved for Mn in GaAs.

Mn substitutes for Ga in a mixture of the Mn<sup>2+</sup> and Mn<sup>3+</sup> oxidation states. The 3*d* electron count is slightly more than 5, which would correspond to a half-filled, fully polarized *d* shell.<sup>7,15,16</sup> Although the occupied Mn 3*d* states lie far below the Fermi level  $E_F$  in photoemission (at about –4.5 eV) they are able to affect the carriers in the GaAs host by producing holes near the As 4*p*-derived valence band maximum and spin-polarizing them.<sup>17–19</sup> The interaction is antiferromagnetic and very efficient, creating very large *g* factors since a single Mn impurity can polarize many carriers. An additional contribution to antiferromagnetism from charge compensated clusters formed by two substitutional and one interstitial Mn atom has recently been proposed.<sup>20,21</sup>

Empty 3*d* states can be probed using soft x-ray absorption<sup>22–24</sup> where optical transitions from the Mn 2*p*<sub>3/2</sub> and 2*p*<sub>1/2</sub> core levels to the Mn 3*d* states are probed at photon energies of about 640 and 650 eV, respectively. In x-ray absorption the 2*p* core hole strongly affects the energy of the 3*d* states and generates an atomlike multiplet splitting.<sup>25</sup> When interpreting core level absorption spectra in terms of ground state electronic states one is faced with the dilemma that the delocalized 3*d* states become localized by the pointlike core hole potential and thus exhibit a mixture of bandlike and localized character. The theoretical model of our x-ray absorption data developed in the following emphasizes the localized character. The delocalized model will be addressed in a separate publication.<sup>26</sup>

We have used transition metals in ZnS as prototypes of wide-gap magnetic semiconductors. For measuring x-ray absorption the core level fluorescence yield is detected instead of the more common electron yield detection. Fluorescence detection has several advantages over electron yield measurements. The longer mean free path of the fluorescence photons, compared to that of the electrons, minimizes the effects of surface contamination. Photon detection also eliminates charging problems and greatly improves the signal/background ratio for dilute impurities. The spectra exhibit considerable fine structure, which makes it possible to determine the tetrahedral crystal field 10*Dq* from the multiplet pattern.

## II. EXPERIMENT

Probing the electronic structure of the dilute transition metals requires a detection method that discriminates against the signal from the semiconductor host. Soft x-ray absorption can be doubly selective by tuning the energy of the absorbed photons to the core level resonance of the transition metal, as well as detecting fluorescence from the same core level. Commonly, secondary electrons are collected which originate from all core holes, including those of the matrix. As efficient fluorescence detector we used channel plates coated with a KBr photocathode and covered by an Al+C filter which efficiently removed the fluorescence from the Zn 3*p* and S 2*p* core levels at about 90 and 160 eV photon energy.

The bulk sensitivity of fluorescence detection (with an absorption length of 160–1000 nm in ZnS over the 400–900 eV range) minimizes the effects of surface contamination. Nevertheless, the samples were freshly cleaved from a single crystal before inserting them into the spectrometer via an introduction lock. An additional problem with high quality ZnS single crystals was charging, which was particularly severe for the 3*d* metals with lower Z (Ti to Cr). This made it impossible to extract electrons, but the detection of fluorescent photons was not affected.

The experiments were carried out at several synchrotron beam lines at the SRC (HERMON, 10 m TGM) and the ALS (BL 4.0, BL 8.0)<sup>27,28</sup> using a newly developed end station for NEXAFS and MCD with fluorescence detection. Most of the data presented are from the ALS BL 4.0 and the rest from BL 8.0. The SRC was used for screening of the crystals. Both ALS beamlines were operated with a resolving power  $E/\Delta E > 5500$  which resulted in a typical energy resolution of 0.1 eV. That is below the calculated intrinsic width of the core levels.<sup>29</sup> Fluorescence count rates/s in the  $10^4$ – $10^5$  range could be achieved at the ALS. Light was incident at 30° from the sample normal with *p* polarization. The fluorescence was detected in a cone with 40° opening, centered at 52° from normal in a plane perpendicular to the plane of incidence (detecting both polarizations equally). A detection angle more grazing than the incidence angle helps making the escape depth shorter than the absorption depth, which is required for obtaining a signal proportional to the absorption coefficient.

In order to obtain high quality single crystals of transition metals in ZnS it was necessary to first purify commercially available raw materials (ZnS and transition metal compounds). These were ground to a powder, mixed, pressed into pellets, and sintered for several days at temperatures of 1000–1100 °C. Chemical transport was used to grow single crystals from the sintered material.<sup>30</sup> It was placed in a quartz tube together with iodine (10 mg/cm<sup>3</sup>) as the transport agent, sealed in vacuum, and heated in a furnace with a temperature gradient from 980 °C to 1000 °C between the two ends of the tube (15 mm apart). Single crystals were obtained after 1–2 weeks with a composition close to that of the starting material.

## III. X-RAY ABSORPTION SPECTRA

The concentration dependence for Mn in ZnS is shown in Fig. 1. Fluorescence detection distorts the response function

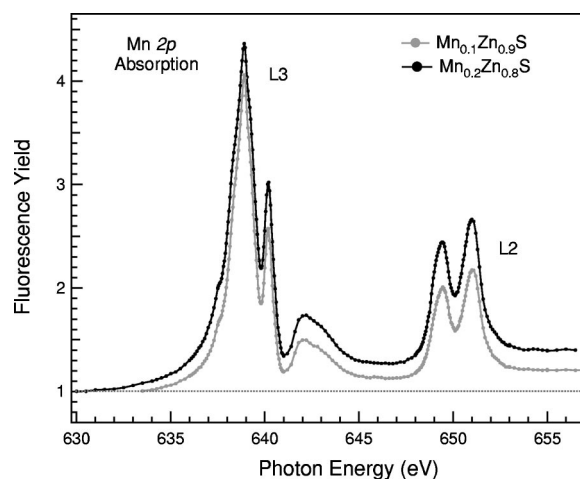


FIG. 1. X-ray absorption spectra for the Mn  $2p \rightarrow 3d$  transitions of Mn in ZnS taken with fluorescence detection, normalized to the pre-edge background. A large signal-to-background ratio achieved by fluorescence detection. The comparison between Mn concentrations of 10% and 20% of the Zn sites shows that saturation and self-absorption are weak for concentrations below 10%, except near the main  $L_3$  peak.

in bulk samples via saturation and self-absorption. Saturation sets in when the absorption is so high that the absorption length becomes comparable to the escape depth or even shorter. In this limit every fluorescence decay produces a detectable fluorescence photon, independently of the absorption coefficient. This happens near the dominant  $2p_{3/2}$  ( $L_3$ ) absorption peak in 3*d* transition metals. Self-absorption occurs for the higher  $2p_{1/2}$  ( $L_2$ ) absorption features whose red-shifted fluorescence is partially absorbed by the lower  $2p_{3/2}$  transition. As a consequence, the  $2p_{1/2}$  features are suppressed relative to the  $2p_{3/2}$  peak. Both of these distortions vanish in the dilute limit where the matrix determines the absorption length, not the impurity. The necessary dilution is explored in Fig. 1, where spectra are shown for two different concentrations of Mn in ZnS with 10% and 20% of the Zn sites substituted by Mn. The overall shapes are quite similar, except for the onset of saturation at the  $2p_{3/2}$  absorption peak in the 20% sample. Therefore we have kept the concentration below 10% with some samples as low as 3%. Note that residual saturation effects for concentrations below 10% could reduce the height of the main  $L_3$  peak, but they would not affect its position or any other peak position. Apart from the onset of saturation effects at 20% Mn concentration there is little evidence of broadening due to interactions between impurities, at least not at the level of the intrinsic linewidth.

Figure 2 gives a systematic series of  $2p \rightarrow 3d$  spectra across the 3*d* transition metal series in ZnS. In general one observes very sharp features, sharper than in previous work on transition metal impurities in ZnS,<sup>23,24,31</sup> ZnSe,<sup>22</sup> and related systems.<sup>32,33</sup> The signal has been normalized to the pre-edge background. Even for 3% of Ti the signal-to-background ratio remains as large as 3:1. The observed features follow the overall trend in the 3*d* series: The  $2p_{3/2}$ - $2p_{1/2}$  spin-orbit splitting increases with the atomic number such that the corresponding multiplets become better separated.

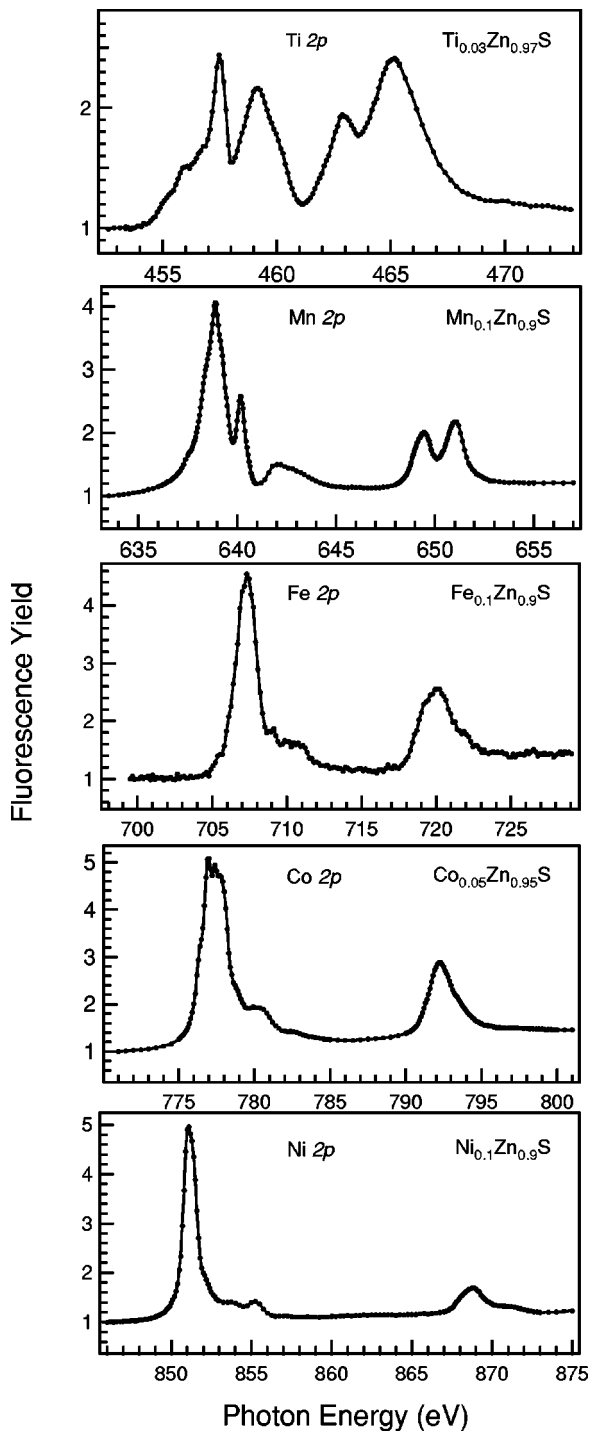


FIG. 2. X-ray absorption spectra of the  $2p \rightarrow 3d$  transitions for a series of transition metals in ZnS.

To our knowledge, only two previous  $L$ -edge NEXAFS measurements of transition metals in ZnS have been published.<sup>23,24</sup> The first shows results for Mn and Co at concentrations of 3%–40%, the second for Mn, Fe, Co, Ni, at concentrations of 1%–50%. Neither of them includes Ti doped ZnS, which is studied here for the first time. In all previous work total electron yield detection was used and the samples were powder samples spread into an indium foil. The energy resolution was around 0.4 eV in both cases. The

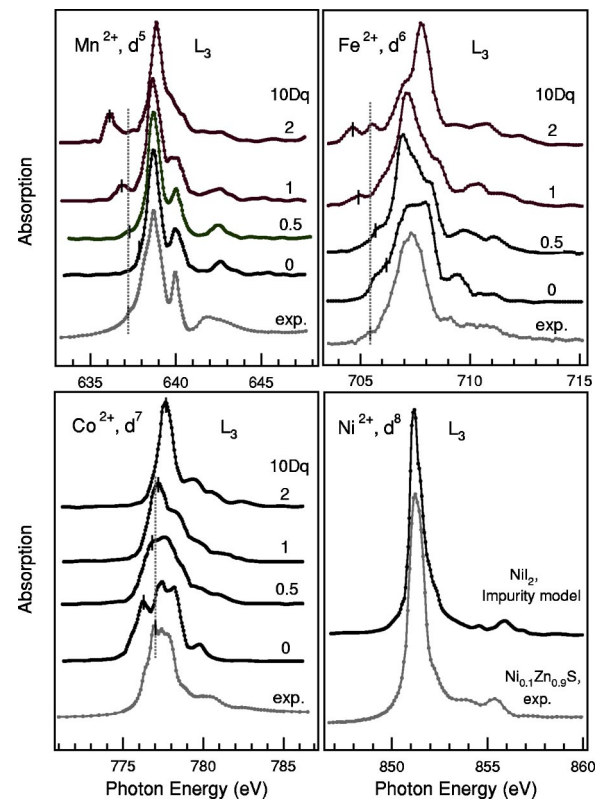


FIG. 3. Determination of the crystal field parameter  $10Dq$  by comparison of atomic multiplet calculations (Ref. 25) and experiment for the  $2p \rightarrow 3d$  absorption spectra. The energy shift of characteristic features (tickmarks) with  $10Dq$  is used to obtain the optimum values given in Table I. For Ni, an impurity calculation for  $\text{NiI}_2$  is shown (Ref. 36).

use of fluorescence detection and single crystals, together with the considerably better resolution in our experiment, makes it possible to distinguish structures that were not resolved in previous measurements, in particular a new pre-edge structure in the  $L_3$  region.

We also measured the missing elements V, Cr but found a substantial background of fluorescence from the Zn  $2p$  edge at 1 keV due to second order light (which could not be filtered out in this experiment).

The spectra are analyzed in Fig. 3 in terms of atomic multiplet calculations in a crystal field with tetrahedral symmetry.

#### IV. ANALYSIS OF THE MULTIPLY STRUCTURE

The multiplet fine structure originates mainly from two effects, the interaction of the  $3d$  electrons with the  $2p$  core hole (including the extra  $3d$  electron excited in the absorption process) and the crystal field at a  $\text{Zn}^{2+}$  site caused by neighboring ions. The two interactions are comparable in magnitude and, therefore, need to be considered together. This is achieved most conveniently in an atomic picture.<sup>25,34</sup> Although the  $3d$  electrons have significant band character in the ground state, they become more localized by their attraction to the pointlike core hole. A discussion starting from the band picture can be found elsewhere.<sup>26</sup>

TABLE I. Characteristic parameters for the  $3d$  electrons of transition metals in ZnS. The tetrahedral crystal field parameter  $10Dq$  is obtained from a fit of our data to multiplets calculated for a  $2+$  ground state (Ref. 25) for the transition metal substituting for  $Zn^{2+}$ . The Pauling electronegativity  $\chi$  is 1.6 for Zn and 2.5 for S.

$3d$ metal	Ti <sup>2+</sup>	Mn <sup>2+</sup>	Fe <sup>2+</sup>	Co <sup>2+</sup>	Ni <sup>2+</sup>
Configuration	$3d^2$	$3d^5$	$3d^6$	$3d^7$	$3d^8$
Electronegativity $\chi$	1.5	1.5	1.8	1.8	1.8
$10Dq$ (eV)		$0.5 \pm 0.25$	$0.7 \pm 0.25$	$0.7 \pm 0.25$	

For the analysis of our data we use atomic multiplet calculations<sup>25</sup> for a tetrahedral crystal field, which is characteristic of substitutional metal atoms in ZnS. There are no calculations of the crystal field effect available for the structure of our samples, which is wurtzite according to recent X-ray diffraction data. Since the nearest neighbor bonding is tetrahedral in both structures one might expect that our analysis still yields the correct magnitude for the crystal field. Starting with a  $3d^n$  ground state, the final state of the absorption process becomes  $2p \ 3d^{n+1}$  with a  $2p$  hole (underlined) and an extra  $3d$  electron. The  $2+$  oxidation state is taken as ground state (see Table I), although a refinement should include a percentage of other configurations, such as a  $3d^{n+1} L$  ground state with a  $3d^{n+2} L$  excited state<sup>22</sup> ( $L$  designates a ligand hole in the S  $3p$  valence band). The addition of other configurations tends to broaden the calculated spectrum<sup>22</sup> rather than introducing extra features. The crystal field, on the other hand, leads to sharp additional peaks by splitting degenerate levels. Some of these peaks shift with energy as the crystal field parameter  $10Dq$  is increased and thus provide an opportunity to delineate  $10Dq$  by matching them to the experimental peak positions (see the tickmarks in Fig. 3). The calculated multiplet structure<sup>25</sup> varies smoothly with the crystal field parameter  $10Dq$  as shown in Fig. 3. Only for very large  $10Dq$  is there a discontinuity due to a transition from a high spin state to a low spin state.<sup>34,35</sup> This happens at  $10Dq=3$  eV for Mn  $3d$  (Ref. 5) and Fe  $3d$  (Ref. 6), a value much higher than the optimum parameters for our data. They are all less than 1 eV (see Table I).

The linewidth in the calculated curves is a combination of a Lorentzian lifetime broadening for the core hole (from 0.16 eV for Mn to 0.22 eV for Co) plus a Gaussian broadening for a typical instrumental resolution (from 0.18 eV for

Mn to 0.24 eV for Co). For the Ni spectrum a 0.3 eV Lorentzian plus a 0.3 eV Gaussian broadening were applied.

For assigning  $10Dq$  in Fig. 3 we select sharp pre-edge features which vary rapidly and systematically with  $10Dq$ . They are indicated by tickmarks above the theory curves of Fig. 3. Although small in intensity and only visible with high resolution, these features are more reliable indicators for  $10Dq$  than the main  $L_3$  and  $L_2$  features, which consist of many unresolved subpeaks in the calculations. Furthermore, the intensity of the main  $L_3$  peak is affected by saturation. The  $L_2$  features are left out in the comparison in Fig. 3 for several reasons. They are attenuated by self-absorption and they are broadened by the extra  $L_2L_3V$  Auger decay channel.

The optimum crystal field parameters resulting from this procedure are listed in Table I. For Ti the appropriate calculations<sup>25</sup> for the Ti<sup>2+</sup> oxidation state are not available. The Ni<sup>2+</sup> calculations<sup>25</sup> do not produce an adequate fit. No matter which  $10Dq$  is chosen, the upper satellite of the  $L_3$  peak at 868.8 eV is missing. Consulting calculations for Ni halides and oxides<sup>36</sup> we noticed that such a satellite appears for low ionicity. The spectrum calculated for the compound with the lowest ionicity considered, NiI<sub>2</sub>, fits our data for Ni in ZnS quite well (Fig. 3). It turns out that the electronegativity of iodine is equal to that of S. Extracting  $10Dq$  would require similar impurity model calculations for the appropriate crystal field (tetrahedral instead of octahedral, and variable  $10Dq$  instead of a fixed  $10Dq=1.5$  eV<sup>36</sup>).

In summary, we show that x-ray absorption with fluorescence detection produces sharp  $2p \rightarrow 3d$  multiplets for transition metal impurities in ZnS and gives a large signal-to-background ratio even with samples as dilute as 3% on the Zn sites. The detailed multiplet structure is used to derive the crystal field by comparison with previous atomic multiplet calculations. Similar measurements should be able to provide electronic structure information on a wider class of magnetic semiconductors, particularly those with wide band gap, as long as multiplet calculations become available for the appropriate crystal symmetry and ionicity.

#### ACKNOWLEDGMENT

This work was supported by the DOE under Contract No. DE-FG02-01ER45917. It was conducted at the SRC (supported by the NSF under Award No. DMR-0084402) and at the ALS (supported by the DOE under Contract No. DE-AC03-76SF00098).

<sup>1</sup>J. K. Furdyna and J. Kossut, in *Semiconductors and Semimetals*, edited by J. K. Furdyna and J. Kossut (Academic, Boston, 1988), Vol. 25.

<sup>2</sup>H. Ohno, A. Shen, F. Matsukura, A. Oiwa, A. Endo, S. Katsunoto, and Y. Iye, *Appl. Phys. Lett.* **69**, 363 (1996).

<sup>3</sup>H. Akai, *Phys. Rev. Lett.* **81**, 3002 (1998).

<sup>4</sup>H. Ohldag, V. Solinus, F. U. Hillebrecht, J. B. Goedkoop, M. Finazzi, F. Matsukura, and H. Ohno, *Appl. Phys. Lett.* **76**, 2928 (2000).

<sup>5</sup>T. Dietl, *Semicond. Sci. Technol.* **17**, 377 (2002).

<sup>6</sup>J. J. Berry, S. H. Chun, K. C. Ku, N. Samarth, I. Malajovich, and D. D. Awschalom, *Appl. Phys. Lett.* **77**, 3812 (2000).

<sup>7</sup>M. Oshima, K. Ono, M. Mizuguchi, M. Yamada, J. Okbayashi, A. Fujimori, H. Akinaga, and M. Shirai, *Int. J. Mod. Phys. B* **16**, 1681 (2002).

<sup>8</sup>S. J. Pearton, C. R. Abernathy, M. E. Overberg, G. T. Thaler, D. P. Norton, N. Theodoropoulou, A. F. Hebard, Y. D. Park, F. Ren, J. Kim, and L. A. Boatner, *J. Appl. Phys.* **93**, 1 (2003).

- <sup>9</sup>T. Dietl, H. Ohno, F. Matsukura, J. Cibert, and D. Ferrand, *Science* **287**, 1019 (2000).
- <sup>10</sup>T. Mizokawa, T. Nambu, A. Fujimori, T. Fukumura, and M. Kawasaki, *Phys. Rev. B* **65**, 085209 (2002).
- <sup>11</sup>H. Toyosaki, T. Fukumura, Y. Yamada, K. Nakajima, T. Chikyow, T. Hasegawa, H. Koinuma, and M. Kawashaki, *Nat. Mater.* **4**, 221 (2004).
- <sup>12</sup>H. Saito, V. Zayets, S. Yamagata, and K. Ando, *Phys. Rev. Lett.* **90**, 207202 (2003).
- <sup>13</sup>S. C. Erwin and C. S. Hellberg, *Phys. Rev. B* **68**, 245206 (2003).
- <sup>14</sup>S. C. Erwin, *Bull. Am. Phys. Soc.* **49**, 403 (2004).
- <sup>15</sup>J. Okabayashi, A. Kimura, O. Rader, Y. T. Mizokawa, A. Fujimori, T. Hayashi, and M. Tanaka, *Phys. Rev. B* **58**, R4211 (1998).
- <sup>16</sup>R. A. Stern, T. M. Schuler, J. M. MacLaren, D. L. Ederer, V. Perez-Dieste, and F. J. Himpsel, *J. Appl. Phys.* **95**, 7468 (2004); O. Rader, C. Pampuch, A. M. Shikin, W. Gudat, J. Okabayashi, T. Mizokawa, A. Fujimori, T. Hayashi, M. Tanaka, A. Tanaka, and A. Kimura, *Phys. Rev. B* **69**, 075202 (2004).
- <sup>17</sup>L. M. Sandratskii and P. Bruno, *Phys. Rev. B* **66**, 134435 (2002).
- <sup>18</sup>L. M. Sandratskii and P. Bruno, *Phys. Rev. B* **67**, 214402 (2003).
- <sup>19</sup>P. Mahadevan and A. Zunger, cond-mat/0309509 v1 (unpublished).
- <sup>20</sup>P. Mahadevan and A. Zunger, *Phys. Rev. B* **68**, 075202 (2003).
- <sup>21</sup>S. C. Erwin and A. G. Petukhov, *Phys. Rev. Lett.* **89**, 227201 (2002).
- <sup>22</sup>C. Kwanghyun, K. Hoon, P. Jonghyurk, S. J. Oh, K. Hyeong Do, M. Han, J. H. Park, C. T. Chen, Y. D. Kim, J. S. Kim, and B. T. Jonker, *Phys. Rev. B* **63**, 155203 (2001).
- <sup>23</sup>K. Lawniczak-Jablonska, R. C. C. Perera, J. H. Underwood, E. M. Gullikson, and R. J. Iwanowski, *Phys. Rev. B* **55**, 10376 (1997).
- <sup>24</sup>W. F. Pong, R. A. Mayanovic, J. K. Kao, H. H. Hseih, J. Y. Pieh, Y. K. Chang, K. C. Kuo, P. K. Tseng, and J. F. Lee, *Phys. Rev. B* **55**, 7633 (1997).
- <sup>25</sup>G. van-der-Laan and I. W. Kirkman, *J. Phys.: Condens. Matter* **4**, 4189 (1992).
- <sup>26</sup>T. M. Schuler, R. A. Stern, J. M. MacLaren, D. L. Ederer, V. Perez-Dieste, F. J. Himpsel, S.-A. Lopez-Rivera, T. A. Callcott (to be published).
- <sup>27</sup>A. T. Young, V. Martynov, and H. A. Padmore, *J. Electron Spectrosc. Relat. Phenom.* **101–103**, 885 (1999).
- <sup>28</sup>J. J. Jia, T. A. Callcott, J. Yurkas, A. W. Ellis, F. J. Himpsel, M. G. Samant, J. Stohr, D. L. Ederer, J. A. Carlisle, E. A. Hudson, L. J. Terminello, D. K. Shuh, and R. C. C. Perera, *Rev. Sci. Instrum.* **66**, 1394 (1995).
- <sup>29</sup>O. Keski-Rahkonen and M. O. Krause, *At. Data Nucl. Data Tables* **14**, 139 (1974).
- <sup>30</sup>V. J. Garcia, J. M. Briceno-Valero, L. Martinez, A. Mora, S. A. Lopez-Rivera, and W. Giriat, *J. Cryst. Growth* **173**, 222 (1997).
- <sup>31</sup>W. F. Pong, R. A. Mayanovic, K. T. Wu, P. K. Tseng, B. A. Bunker, A. Hiraya, and M. Watanabe, *Phys. Rev. B* **50**, 7371 (1994).
- <sup>32</sup>A. Kisiel, A. I. Ali-Dahr, P. M. Lee, G. Dalba, P. Fornasini, and E. Burattini, *Phys. Rev. B* **44**, 11075 (1991).
- <sup>33</sup>J. Oleszkiewicz, M. Podgomy, A. Kisiel, and E. Burattini, *Phys. Rev. B* **60**, 4920 (1999).
- <sup>34</sup>F. M. F. de-Groot, *J. Electron Spectrosc. Relat. Phenom.* **67**, 529 (1994).
- <sup>35</sup>G. van der Laan, B. T. Thole, G. A. Sawatzky, and M. Verdaguer, *Phys. Rev. B* **37**, 6587 (1988).
- <sup>36</sup>G. van der Laan, J. Zaanen, G. A. Sawatzky, R. Karnatak, and J. M. Esteve, *Phys. Rev. B* **33**, 4253 (1986).